Journal of Engineering Science and Technology
Vol. 12, No. 3 (2017) 667 - 685

SQUEEZE FILM DAMPER EFFECT ON VIBRATION OF AN UNBALANCED FLEXIBLE ROTOR USING HARMONIC BALANCE METHOD

FENG HE[1], SAEID DOUSTI[2,*], PAUL ALLAIRE[2], MAJID DOUSTI[3]

[1]Rotating Machinery and Controls Lab, Mechanical and Aerospace Engineering Department, University of Virginia, Charlottesville, VA, USA
[2]Rotor Bearing Solutions International, LLC, Charlottesville, VA, USA
[3]Faculty of Engineering, Zanjan University, Zanjan, Iran
*Corresponding Author: Saeid.Dousti@rotorsolution.com

Abstract

In this paper, an effective tool based on harmonic balance method to assess the forced response of these systems under parametric changes is developed. A flexible rotor with multiple masses supported on a squeeze film damper at one end is investigated and modeled using finite element method. The forced response of this asymmetrically supported system is calculated using the harmonic balance method with a predictor-corrector procedure by changing unidirectional loads, stiffness of centering spring of the damper and the gyroscopic effects of the disks. It is observed that under large unbalance forces, jump phenomenon occurs due to the nonlinear forces of SFD which indicates the presence of multiple harmonics within the response of the SFD operating at high eccentricity ratios and shows the insensitivity of the damper to surrounding gyroscopic variation.

Keywords: Squeeze film damper, Unbalance response, Harmonic balance method.

1. Introduction

Squeeze film dampers are the shock absorbers of turbomachinery. The trend of high-speed and high-power density of modern turbines requires reliable operating conditions avoiding vibration and stability problems. Squeeze film dampers, due to their ability to improve those performances, has been widely employed in these machines for over five decades [1-3]. Meanwhile, the nonlinearity introduced within the application continues to draw the interests of researchers and engineers in the field of rotordynamics.

Nomenclatures

C	Damping matrix, $\mathrm{N.s/m}$
c	Damper radial clearance, m
e	Eccentricity ratio, $e = \sqrt{x^2 + y^2}$, m
F	External force vector, N
f_x, f_y	Damper forces, N
G	Gyroscopic matrix, $\mathrm{N.s^2/m}$
h	Film thickness, $h = c - x\cos\varphi - y\sin\varphi$, m
I_p	Polar inertia of disk, $\mathrm{N.s^2/m}$
K	Stiffness matrix/stiffness, $\mathrm{N/m}$
k	Number of harmonics included
L	Damper axial length, m
M	Mass matrix, kg
M_2	Ball bearing mass, kg
p	Pressure, Pa
R	Damper radius, m
r	Radial direction of polar coordinate
s	Step length to ensure the continuity
T	Tangential direction of polar coordinate
t	Time, s
U	Unbalance, g-mm
X_o	Constant terms in Fourier series, m
X_{ci}	Cosine terms of the Fourier coefficients with ω_i, m
X_{si}	Sine terms of the Fourier coefficients with ω_i, m
x, y	Components of Cartesian coordinate/displacement, m
$\bar{x}, \bar{y}$	Components of Cartesian coordinate/displacement, $\bar{x} = \frac{x}{c}, \bar{y} = \frac{y}{c}$
z	Axial direction, m

Greek Symbols

ε	Eccentricity ratio
μ	Lubricant viscosity, Pa. s
ρ	Density, $\mathrm{Kg/m^3}$
φ	Angle in polar coordinate, rad
Ω	Rotational speed, rpm
ω_i	*i*th frequency included for analysis, $\mathrm{rad/s}$

Subscripts

A	Integer, 1,2
B	Integer, 1,2
FL	Fourier coefficients of linear external forces
FNL	Fourier coefficients of nonlinear external forces
I	Integer, number of harmonics
J	$\sqrt{-1}$
1	Linear part
2	Nonlinear part

It is a common practice to assume that the journal in squeeze film damper whirls in a centered circular path with the same frequency as that of the shaft

rotation, namely, Circular Centered Orbit (CCO). Gunter et al. obtained linearized coefficients of SFDs used in aircraft engines. Similarly, San Andres and Vance [3] examined the force coefficients of an open-ended damper executing off-centered circular orbits with small amplitudes. More recently, Ertas et al. [4] applied linearized coefficients method to model a damper for unbalance response analysis of a rigid rotor. The presentation of SFD's nonlinear forces with linear coefficients is limited to simple rotor-bearing systems and small motion ranges.

To understand the complete characteristics of the nonlinear forces, Taylor [5] and Cookson [6] modeled the damper forces with a fourth order Runge-Kutta integration method to find the nonlinear response of a rotor-bearing system supported on centered, short and off-centered SFDs. With the same procedure, Sykes and Holmes [7] achieved the effects of bearing misalignment on the response of a damper supported rotor, and captured the nonlinear jump phenomenon under different cavitation pressures. Although the direct integration of the damper force in the time domain can include a complete model for rotordynamic analysis, the execution is time consuming, especially for large order systems.

Nataraj and Nelson [8] avoided the disadvantage in time domain by assuming that the displacement has trigonometric form and adopting Trigonometric Collection Method (TCM) for the analysis of uncentered squeeze dampers supporting an axially symmetric rotor. Zhao et al. [9] extended the method to a rotor with 6-DOFs supported on two short squeeze film dampers for both forced response and stability analysis. The convergence of the nonlinear iteration was improved with initial variables having a linear polynomial form. Shiau and Jean [10] used the Harmonic Balance Method (HBM), which has the same displacement form as TCM, to obtain periodic responses of large order nonlinear systems. Their analysis indicated the presence of ultra-sub, sub, super and ultra-sup harmonic components in the results. Similarly, Hahn and Chen [11] obtained the dynamics of a multi-DOFs rotor-bearing system, also using the HBM. The rotor-bearing systems documented above are limited to simple rotors with symmetric bearings. Bonello, Brennan, and Holmes [12], in the discussion of nonlinear modeling of rotordynamic systems with squeeze film dampers, modified the HBM by introducing receptance matrices between displacements and forces and applied the approach to an over-hung rotor. Later, the method was employed to an aeroengine rotor for forced response and stability analysis [13], without including the gyroscopic effects.

The journal inside the squeeze film damper is prevented to rotate. In the lack of rotational lift off motion, a centering mechanism is utilized [14]. This centering mechanism (or spring) provides supporting stiffness and dictates the effective damping property of SFD. Dousti et al. [2, 14] modeled the dynamic behaviour of elastomer O-ring seals as a centering element of SFDs. The use of O-ring seals, as centering spring in addition to their sealing purposes, is more practical in low weight rotors. In larger machines a flexible structure or mechanical spring plays this role. The impellers (disks) dictate the majority of shaft weight and often are considered solid with natural frequencies much higher than those of the rotor's [15]. The heavy load on SFDs can violate the CCO assumption.

An extensive experimental study is conducted by San Andres [16, 17] to show the importance of inertia effects in squeeze film dampers. Dousti also showed the effect of inertia and its appearance in groove SFDs [18]. Adilleta and Della Pietra

[19, 20] provided a comprehensive review of the relevant analytical and experimental work conducted on SFDs.

In the present study, the Harmonic Balance Method is used in the dynamic analysis of a flexible rotor with a finite element model. An improved iteration method with predictor-corrector procedure is applied to a condensed set of equations of motion to improve the computational efficiency. The forced system response under different parameters, such as external loads, supporting stiffness and gyroscopic effects, are investigated to show the influence of the squeeze film damper.

2. Rotor Dynamic Model

Equations of motion of a SFD equipped flexible rotor can be expressed as

$$[M]\ddot{x}(t) + [C + \Omega G]\dot{x}(t) + [K]x(t) = [F(t)] \tag{1}$$

where $x(t)$ is displacement vector having N components, with N the number of the degrees of freedom of the entire system.

In the above equation, $F(t)$ is the external forces acting on the system, including both linear and nonlinear forces. The linear part consists of the unbalance forces and gravity. The nonlinear effects for the current system come from the hydrodynamic forces of SFD.

The HBM approach approximates the displacements as the summation of components with different frequency contents, indicated as

$$x(t) = X_0 + \sum_{i=1}^{k}[X_{ci}\cos(\omega_i t) + X_{si}\sin(\omega_i t)] \tag{2}$$

Substituting the above equation into Eq. (1) and balancing the frequencies on the sides yield new equations in frequency domain as

$$[K]X_0 = \tilde{F}_{const} \tag{3}$$

$$([K] - \omega_i^2[M])X_{ci} + \omega_i[C + \Omega G]X_{si} = \tilde{F}_{cos} \tag{4}$$

$$([K] - \omega_i^2[M])X_{si} - \omega_i[C + \Omega G]X_{ci} = \tilde{F}_{sin} \tag{5}$$

where $\tilde{F}_{const}$, $\tilde{F}_{cos}$ and $\tilde{F}_{sin}$ are the Fourier coefficients of the external forces of the rotor-bearing system, representing constant, cosine and sine terms, respectively. To this point, the original implicit equations of motion in the time domain are replaced with the new implicit linear algebraic equations in the frequency domain. This increases the total number of the unknowns from N to $N(2k+1)$. To eliminate the number of unknowns to be solved for directly, a similar condensation procedure introduced by Hahn [11] is applied to Eqs. (3), (4), and (5) in complex form for simplicity. Based on this method the complex vector R is defined as

$$R = \begin{cases} X_0, & i = 0 \\ X_{ci} + j\,X_{si}, & i = 1,2,\ldots\ k \end{cases} \tag{6}$$

Rearranging Eqs. (3), (4), and (5) by separating the linear and nonlinear parts gives leads to the following equations for each frequency,

$$\begin{bmatrix} P_{11} & P_{12} \\ P_{21} & P_{22} \end{bmatrix}_i \begin{Bmatrix} R_1 \\ R_2 \end{Bmatrix}_i = \begin{Bmatrix} F_L^1 \\ F_L^2 \end{Bmatrix}_i + \begin{Bmatrix} 0 \\ F_{NL}^2 \end{Bmatrix}_i \tag{7}$$

$$[P_{\alpha\beta}]_i = [K_{\alpha\beta}]_i - \omega_i^2 [M_{\alpha\beta}]_i - j\omega_i [C_{\alpha\beta}]_i \tag{8}$$

From Eq. (7), a condensed equation will be available for the displacement of nonlinear part $\{R_2\}$ as

$$\{R_2\}_i = [U]_i^{-1}(\{F_{NL}^2\}_i - \{V\}_i) \tag{9}$$

where the terms on the right hand side are

$$[U]_i = (-[P_{21}][P_{11}^{-1}][P_{12}] + [P_{22}])_i \tag{10}$$

$$\{V\}_i = ([P_{21}][P_{11}^{-1}]\{F_L^1\} - \{F_L^2\})_i \tag{11}$$

An iterative procedure will be carried out on the *n* DOFs of the nonlinear parts only, which is usually fewer than the *N* DOFs of the entire system. The solution of the linear components $\{R_1\}$ is available readily from Eq. (7) when the $n(2k+1)$ unknowns of $\{R_2\}$ are obtained. Thus, the main effort required to implement the Harmonic Balance Method is only conducting the iterations to get the displacements of the nonlinear parts. The efficiency of this iterative algorithm dominates the overall computational speed of this method. One of the major factors influencing the speed is the initial guess. The further away the initial values are from the solution, the longer it takes for the iterative procedure to convergence. An inappropriate initial guess may also lead to divergence. The idea of homotopy [21] can be adopted to get closer initial guess for the first solution. For this particular problem of rotordynamic systems, the unbalance responses without nonlinear components (using linearized squeeze film damper coefficients) are ideal initial guesses. Even for unsupported-damper systems with the consideration of gravity, the responses from a linearized system analysis without gravity can be the first solution set. It is then followed by a piecewise increment to full-load. For each step of iteration, a root finding method such as the Newton-Raphson is utilized.

A predictor-corrector procedure is employed to find the next solution, once the first iteration results are available. In the current analysis, the predictor of the next step is obtained using a pseudo-arc length continuity model [22] as given in Eq. (6). This predictor is then corrected with Newton-Raphson method.

$$\sum_{l=1}^{n} \left(y_l - y_l(s_j)\right) \frac{dy_i(s_j)}{ds} + \left(\lambda - \lambda(s_j)\right) \frac{d\lambda(s_j)}{ds} = ds \tag{12}$$

Together with Eq. (5), the total $n(2k+1)+1$ unknowns are found by solving $n(2k+1)+1$ equations, with ensured continuity of all the solutions over interested range of parameter λ.

Another factor affecting the computational results during the iteration is the number of frequencies included in the Harmonic Balance Method. In present analysis, a group of harmonics from sub- to super- is included for the initial guess (or the predictors). Then, based upon their component amplitudes, as compared to the damper clearance, the important components will be kept for the corrections within the current step.

3. Squeeze Film Damper Model

Figure 1 depicts the side view of a squeeze film damper. The squeeze film lubricant is considered to be Newtonian, laminar, and with inertia included. We follow the method by Dousti et al. [23, 24] by adopting the short bearing assumption in order to simplify the solution of Reynolds equation. Thus, the reduced Reynolds equation with the inclusion of temporal inertia which is pertinent to SFDs reads

$$\frac{\partial}{\partial z}\left(h^3\frac{\partial p}{\partial z}\right) = 12\mu\frac{\partial h}{\partial t} + \rho h^2\frac{\partial^2 h}{\partial t^2} \tag{13}$$

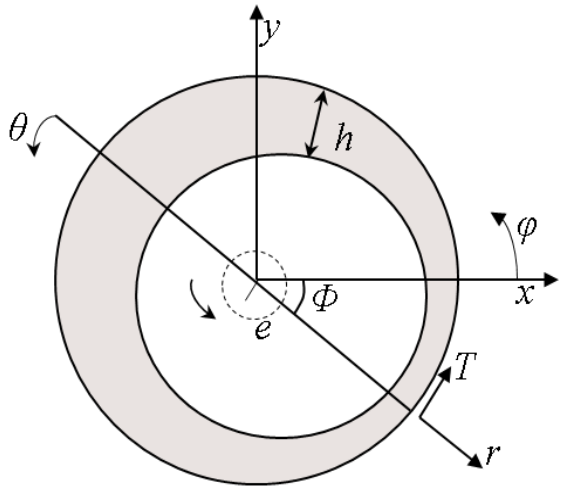

Fig. 1. Axial view of SFD.

The solution of the above equation, $p(\varphi, z)$, is analytically available [23]. Additionally, Dousti et al. calculated the pressure profile and the generated forces using a CFD technique [25]. Be noted that in this study, the cavitation phenomenon is considered by suppressing the negative part pf pressure profile. Thus, the nonlinear hydrodynamic forces generated by the damper are

$$\begin{Bmatrix} f_x \\ f_y \end{Bmatrix} = \int_0^L \int_0^{2\pi} \begin{Bmatrix} p(\varphi, z)R\cos\varphi\, d\varphi\, dz \\ p(\varphi, z)R\sin\varphi\, d\varphi\, dz \end{Bmatrix} \tag{14}$$

Note that the harmonic balance method is carried out in frequency domain instead of the time domain. To avoid complicated direct Fourier transformation of Eq. (9), the nonlinear forces are integrated in time domain before being transferred to the frequency domain. With this alternating procedure, more complex damper models, such as piston-ring or O-ring sealed dampers, can be applied without much additional effort using a similar method.

To this point, the overall calculation process for the forced response of squeeze film damper supported systems using harmonic balance method is displayed as shown in the flow chart in Fig. 2.

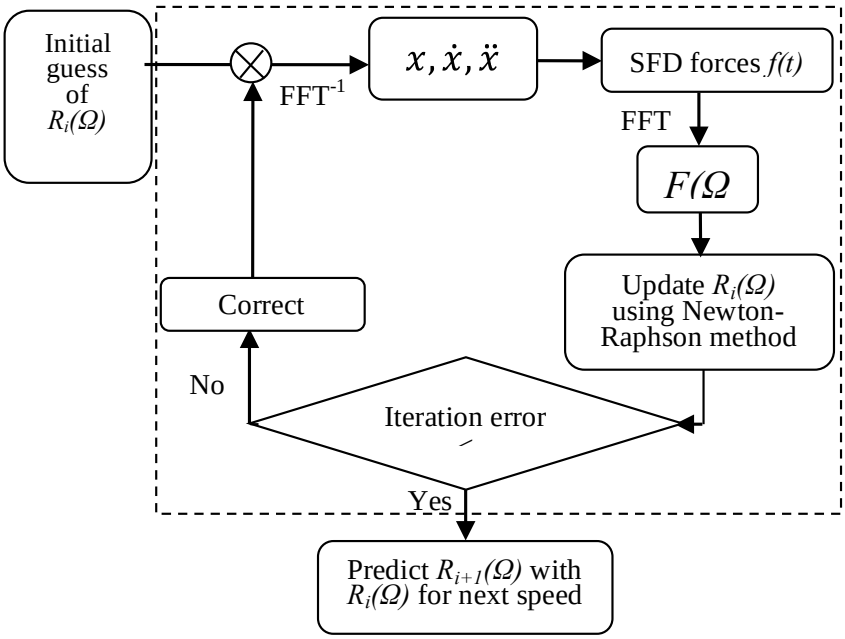

Fig. 2. Flow chart of HBM for *i*th speed.

4. Application to a Flexible Rotor

The aforementioned methodology is applied to a flexible rotor with three disks. The rotor is modeled using finite element method as depicted in Fig. 3. The rotor, having 24 elements, is supported on two identical ball bearings (*Brg1* and *Brg2*), which have stiffness around 1.05e8 N/m. *Brg2*, as shown in the figure, is connected in series to a centered squeeze film damper. The geometry and operating conditions of the damper are listed in Table 1.

Three identical disks, D_1, D_2 and D_3, with $M_D = 3.4$ kg and $I_p = 9.3e-3$ kg. m^2 each, are mounted on the shaft. The ball bearings are assumed to have very high stiffness compared to the squeeze film damper. The damper is considered to have two translational DOFs along x, y directions only and is not misaligned. The overall system has 100 DOFs from the rotor and 2 additional from the damper. Based on Eq. (9), the number of the equations required to be solved iteratively is $2(2k+1)$, where k equals the number of the included harmonics.

In this section, the dimensionless displacement in the squeeze film damper

$$\varepsilon = \frac{\sqrt{x^2+y^2}}{c} \tag{15}$$

is reported in Figs. 4-19. In Eq. (15), c presents the SFD clearance. Different parameters are varied in order to investigate the behaviour of squeeze film damper under different operating conditions [26-28].

Table 1. Damper geometry and operating conditions.

Journal Diameter (mm)	**76.2**
Radial Clearance (mm)	**0.254**
Axial Length (mm)	**25.4**
Lubricant	**ISO VG 32**
ρ **= 865 kg/m^3**	$\mu = 0.028$ **Pa. s**

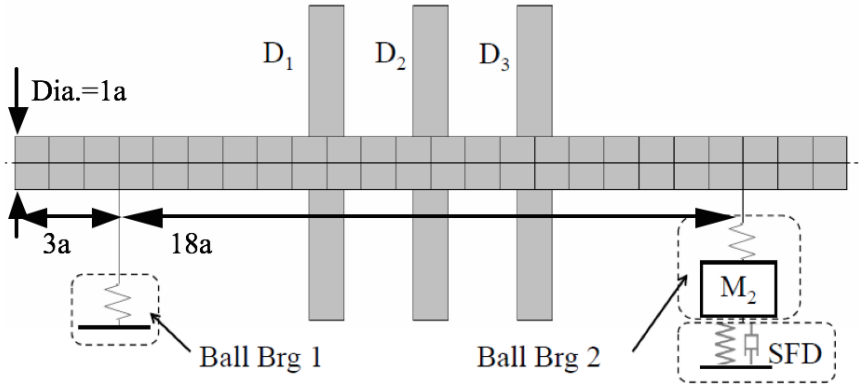

Fig. 3. Finite element model of a flexible rotor, *a*=25.4 mm.

4.1. Forced response with varying unbalance

The responses of the damper to unbalance applied at the locations of three disks are calculated. The amplitude *U* and phase angle of the unbalances are applied to one disk only for each calculation as 431.9 g-mm and 0 degrees, respectively. As depicted in Fig. 4, the critical speeds and their amplitudes for the three cases are quite similar, with the largest amplitude for unbalance on disk 2 and the least on disk 1. This indicates that the squeeze film damper is more sensitive to unbalance on disk 2 than the similar unbalance on other disks.

With larger unbalance (503.9 g-mm), the SFD Response starts to jump, as shown by Figs. 5 to 7. The jump happens between 3,890 and 4,200 rpm for these cases. The speed difference between start-up and coast-down is the largest with 180 rpm when the unbalance is located on disk 2, as compared to 110 rpm for unbalance in disk 3 and 97 rpm for unbalance in disk 1. The corresponding hysteresis area in Fig. 6 is the largest. This implies that the squeeze film damper is the most responsive to unbalance in disk 2.

Note that the responses shown in Figs. 5 to 7 are excited by unbalances on disks only, without considering other external forces. Thus, the justification for the observed hard and soft spring effects of the above nonlinear jump phenomenon is the excessive unbalances. Figure 8 displays the FFT of the response at 3,990 rpm during start-up for unbalance on disk 2. The super-harmonics of the 3x component starts to appear along with the synchronous component.

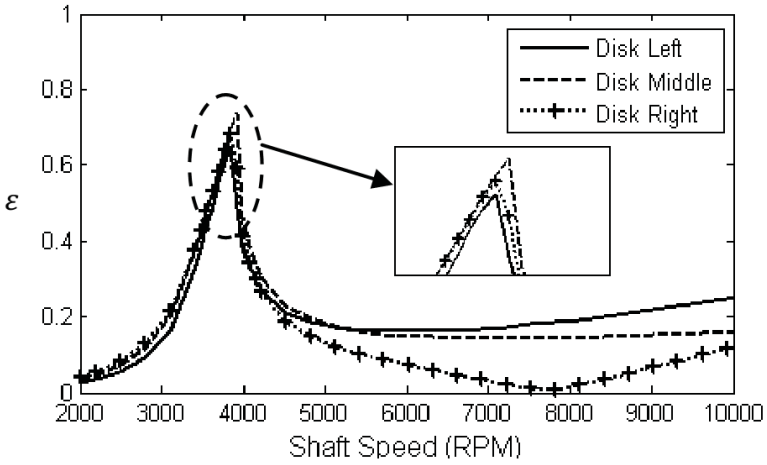

Fig. 4. SFD response, *U*=431.9 g-mm.

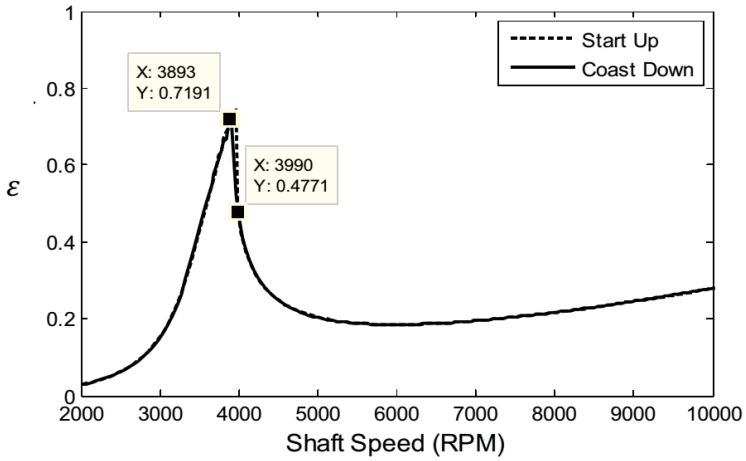

Fig. 5. SFD response, *U*=503.9 g-mm on disk 1.

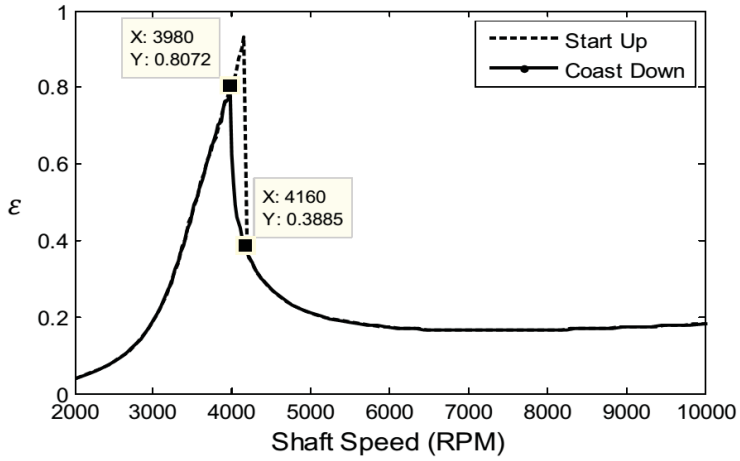

Fig. 6. SFD response, *U*=503.9 g-mm on disk 2.

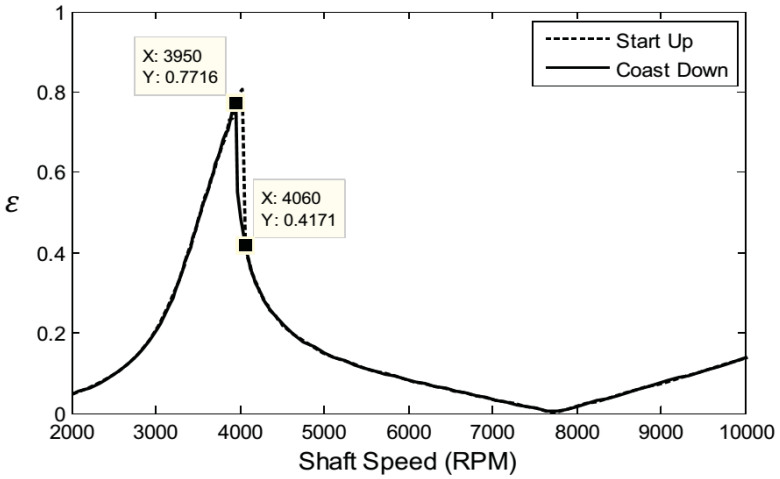

Fig. 7. SFD response, *U*=503.9 g-mm on disk 3.

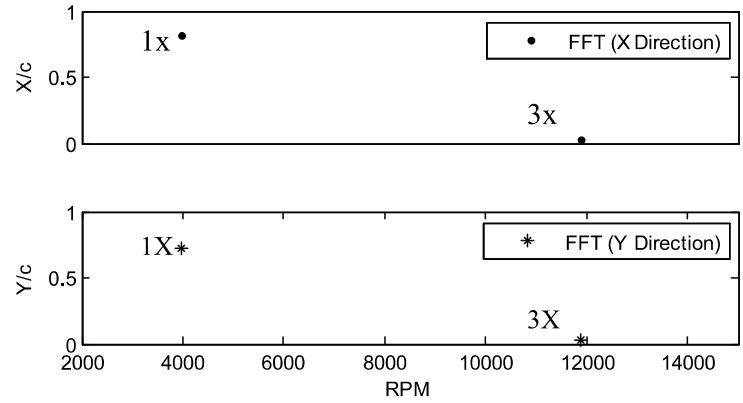

Fig. 8. FFT of response at 3990 rpm, with unbalance on disk 2.

4.2. Forced responses with unidirectional loads

The unidirectional loads are applied by including the gravity forces of the rotor shaft and disks. Compared to the previous cases without gravity loads, the SFD operates eccentrically and exerts more nonlinear forces.

With the same unbalance of 431.9 g-mm on disk 2, Fig. 9 provides the comparison between rotor response with and without loads at location of disk 2. The maximum amplitude of the response with load at the critical speed is quite similar to the case without load. Nevertheless, at rotational speeds other than the critical speed, the difference between cases with and without unidirectional gravity load is accented, i.e., the vibrations amplitude with the inclusion of the gravitational force is higher. This result displays some evidences for the nonlinearity of the squeeze film damper force with displacement. The nonlinear behaviour of SFD is also responsible for the jump phenomenon in Fig. 9. Figure 9 also illustrates the sensitivity of the jump to gravitational force. By neglecting the

effect of gravity on the system, no jump is predicted once a 431.9 g-mm unbalance is mounted on disk 2. Only by increasing the unbalance value to 503.9 g-mm on disk 2, jump appears in the system. However, once the effect of gravitational force is included in the analysis, jump phenomenon occurs even with 431.9 g-mm unbalance on disk 2.

The effect of varying unidirectional loads is investigated by applying an additional downward force at the location of disk 3. The magnitude of this force is varied from 1 up to 16 times the weight of the system. The unbalance of 431.9 g-mm is considered on disk 2 at 0 degree phase angle and Fig. 10 displays the responses to various loads.

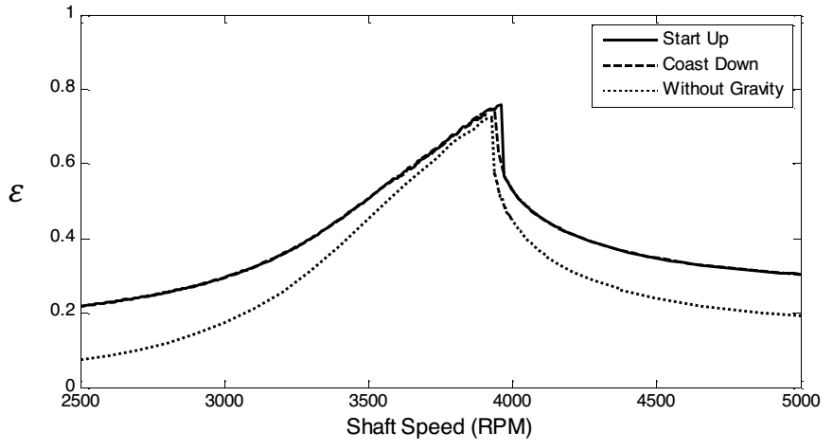

Fig. 9. SFD response with load, *U*=431.9 g-mm on disk 2.

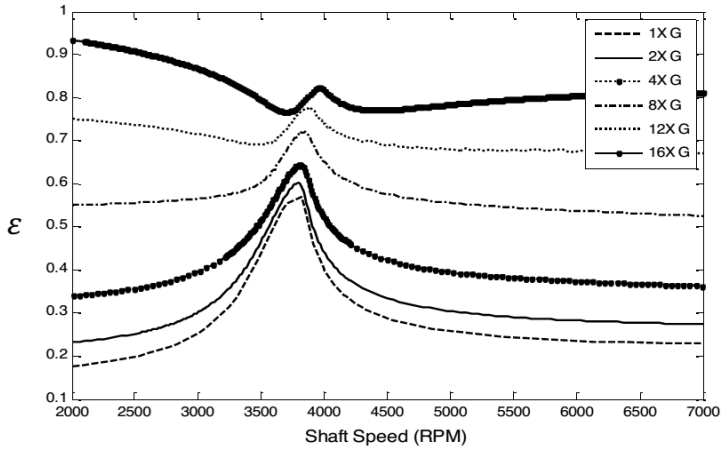

Fig. 10. SFD response with varying loads on disk 3.

As expected, higher loads push the damper to a more eccentric region. The first critical speeds, as is shown in Fig. 10, shifts to the right as loads increase, which is due to higher loads applied by damper in higher eccentricity ratios. By increasing the unidirectional load, the resonance amplitude of vibration decreases.

The amplitude of vibration, when the external load increases to 16xG, is the highest for lower rotational speeds 2000 rpm. Within low operating speed region, the dynamic forces are not large enough to lift off the journal effectively. The increasing speed, although lifts the journal upward somehow, but cannot pull the damper out of high eccentric region that prevents responses with large amplitude. This fact of increasing nonlinearity with loads can also be observed from the shape change of damper orbits as well. Fig. 11 depicts the orbits at 7,000 rpm for increasing unidirectional 16xG. The shapes of the orbits change from an off-centered circle to an ellipse with shrinking amplitude. The non-circular shape implies that multiple harmonics are present for large static loads, which can be confirmed by the FFT in Fig. 12.

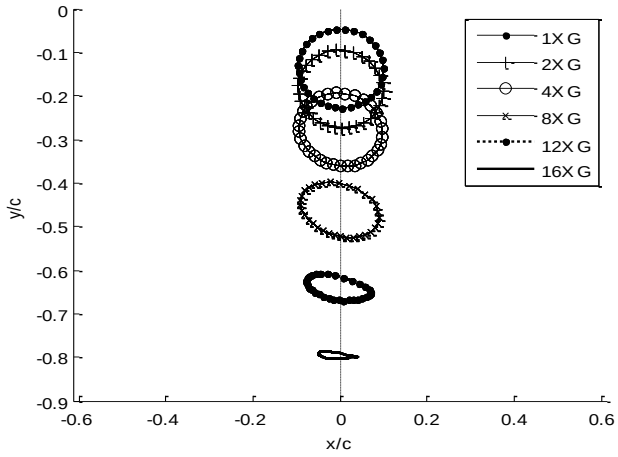

Fig. 11. Orbits at 7000 rpm, with varying loads on disk 3.

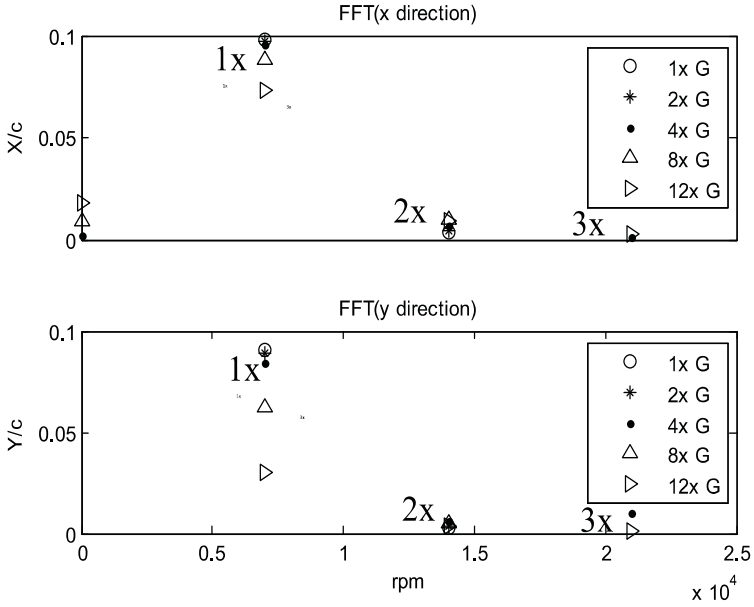

Fig. 12. FFT of orbits (7000 rpm) with varying load.

The zero frequency component in the y direction, which is shown by the offsets of the orbits in Fig. 11, is not included in the FFT plots. The appearance of a zeroth component in the x direction, which is also illustrated in Fig. 11, implies that the center of orbit becomes eccentric not only in y direction, but also displaces in x direction as well. The 1x component in x direction is present for all the cases, however, its amplitude decreases with the growing unidirectional static loads. Meanwhile, the increasing static loads lead to an excitation of the 2x and 3x harmonics within the unbalance response results and produce non-circular orbits as are shown in Fig. 11.

4.3. Stiffness of centering spring

To evaluate damper responses with a varying stiffness of centering spring, the unbalance is kept constant as 431.9 g-mm on disk 2. Both cases with and without the gravitational force are examined.

Case 1. Varying spring stiffness without gravity: Figure 13 displays the responses for spring stiffness ranging from 11.3 N/m to 1130 N/m without gravity inclusion. As the centering spring stiffness increases, the effective damping drops and increases the critical speed, however, not to the extent that the linear model predicts [1].

As shown in Fig. 13, the amplification factor is smaller than 2.5 for the softer centering spring. This indicates that the squeeze film damper acts more effectively without the restriction enforced by centering spring. For speeds above 4,100 rpm, the damper with low centering spring stiffness, on the other hand, operates with larger amplitudes. This observation is quite similar to results with base excited flexible rotor vibrations for frequencies beyond the first critical.

Case 2. Varying spring stiffness with gravity: Figure 14 shows the response of squeeze film damper with centering spring stiffness ranging from 170 to 1130 N/m with the inclusion of gravitational force. As the centering spring stiffness decreases, the damper, as expected, operates at larger eccentricity ratio, similar to the cases with increasing unidirectional loads, however, the amplitude of the vibrations decreases to the level that the resonance peak diminishes completely.

Comparing the graphs in Fig. 14 with those of Fig. 13, the responses with a hard centering spring have a slightly higher first critical speed and amplitude; e.g., the critical speed for K=1130 N/m is 3,800 rpm with dimensionless amplitude of 0.58, which is larger than the amplitude of vibration at 3,790 rpm for the cases without gravity consideration. For both cases, the system is shown to be well-damped with soft centering springs by the evidence of the disappearance of critical speed for centering spring stiffness values less than 282.5 N/m.

For the rotor operating with speeds below 3,000 rpm, the gravity effect dominates the total response for soft centering spring supports and results in high eccentricity operation, which excites the super harmonics as expected. Figure 15 depicts a flat orbit at 2,000 rpm with spring stiffness of 170 N/m. The orbit has small amplitude, indicating rather large hydrodynamic forces acting on the journal. A larger displacement in x direction than y shows that the damper generates higher forces along y direction, exhibiting the high asymmetry of the damper. Also, the FFT of the y direction response contains multi-harmonics

including the 0^{th} (not shown in Fig.16), 1x, 2x and 3x, as compared to the x direction response which has the 0^{th} and 1x component only.

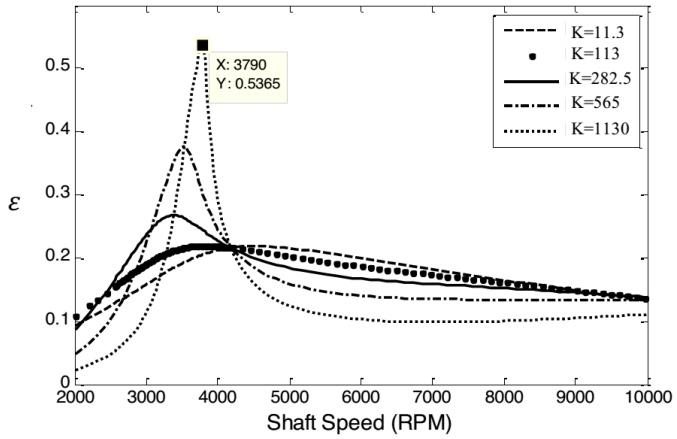

Fig. 13. SFD response without gravity and varying spring stiffness.

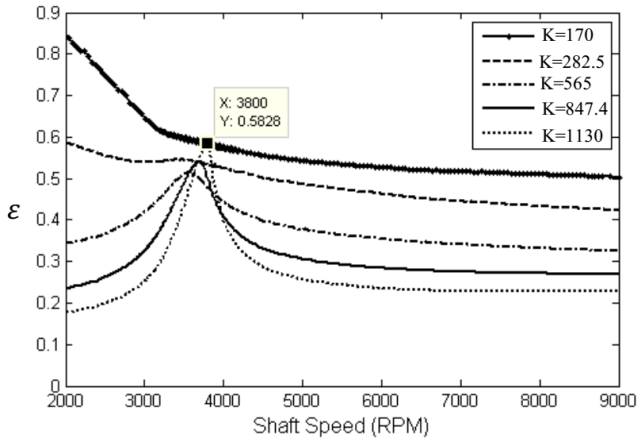

Fig. 14. SFD response with gravity and varying spring stiffness.

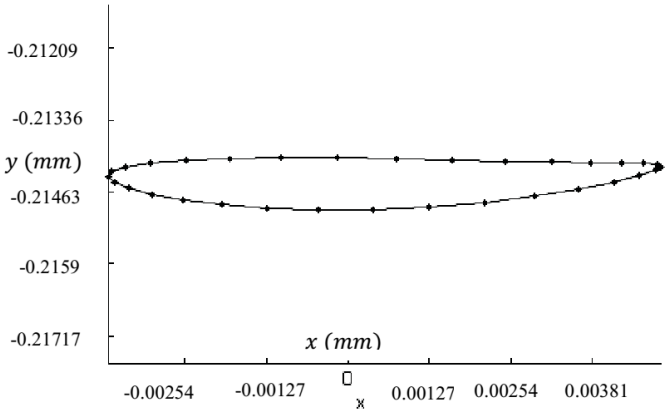

Fig. 15. Orbit at 2000 rpm, *K*=170 N/m.

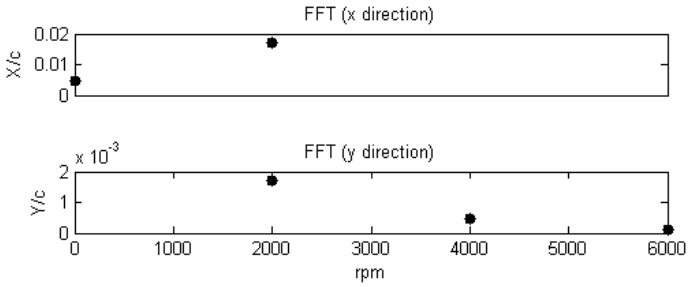

Fig. 16. FFT of response at 2000 rpm, *K*=170 N/m.

4.4. Gyroscopic effects of disks

The gyroscopic matrix of each disk (as the dominant source of gyroscopic effect) is dependent on the polar moment of inertia, I_p, of the disk as

$$G = \begin{bmatrix} 0 & I_p \\ -I_p & 0 \end{bmatrix} \tag{16}$$

The gyroscopic effect is not exclusive to disks but also in other rotating structures like beams, where a vibrational motion along the rotation line exists [29].

Thus, the disk gyroscopic effects on the force response of the SFD are investigated by varying the polar moment of inertia, I_p. An unbalance of 288 g-mm is retained on disk 2 and the gravity effect is not included. The centering spring stiffness is maintained at 282.5 N/m. Figures 17 through 19 display the eccentricity of the journal in SFD for the varying polar moment of inertia from 1x to 16x of nominal value for each disk, i.e., $I_p = 9.3e-3$ kg. m^2.

Figure 17 shows the SFD response for the polar moment of inertia varied on disk 1, which is the furthest from SFD end. It is observed that the smallest inertia results in the maximum response at the damper for speeds less than the respective critical speed. This trend is reversed above the critical speed. By increasing the disk polar inertia, the first critical speed shifts to the right and results in higher resonance amplitude. This shift is justified by the hardening effects of the gyroscopic terms on the first forward mode of the system. In addition, due to the stiff ball bearing at left end, the conical mode of the system is more likely to be excited by disk 1 than the other two, as it locates furthest to the damper.

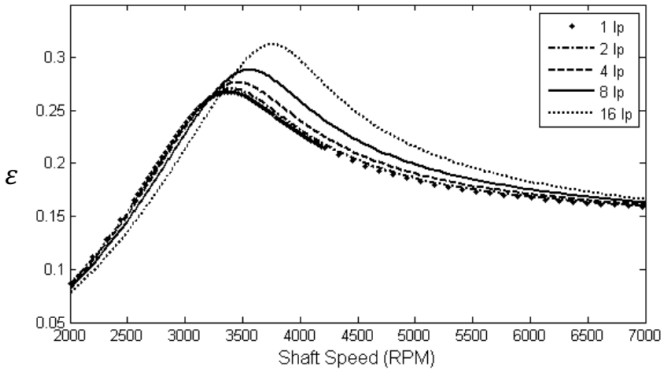

Fig. 17. Response with varying inertia of disk 1.

With the same varying range of the disk polar moment of inertia, Fig. 18 depicts the damper force responses corresponding to the inertia variation in disk 2. The amplitude of all responses is quite similar for operating speeds less than 3,000 rpm. The largest gyroscopic term produces the highest amplitude around the first critical speed and it becomes the lowest for speeds above 4,000 rpm. In contrast to the previous cases, the first critical speeds with studied range of polar moment of inertia of disk 2 are identical, with only a slight increase of the amplitude.

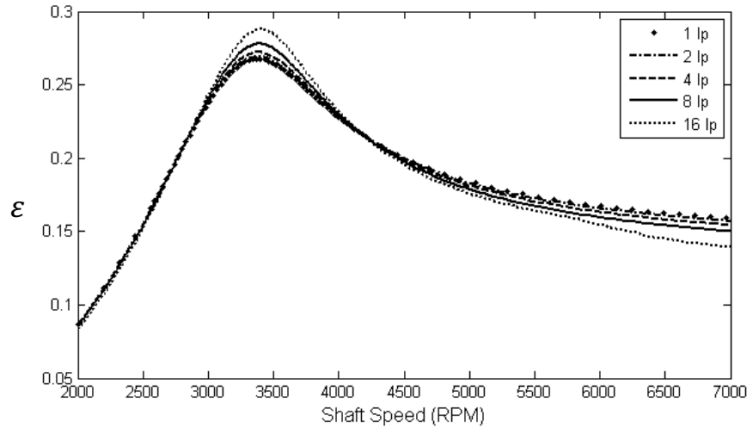

Fig. 18. Response with varying inertia of disk 2.

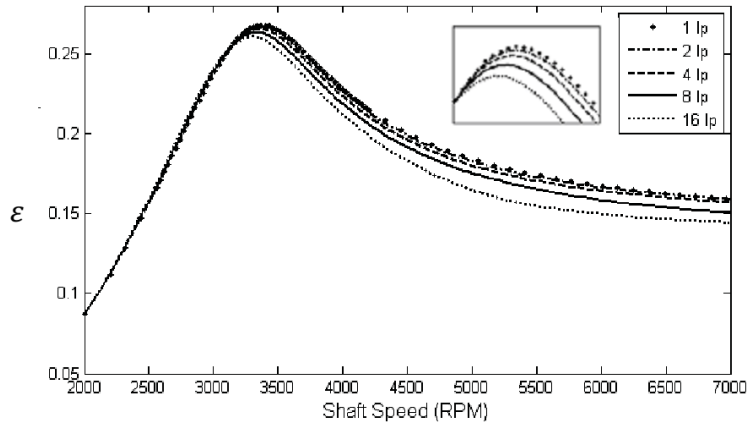

Fig. 19. Response with varying inertia of disk 3.

For the variation of the polar moment of inertia of disk 3, the SFD acts similarly to the second studied case for speeds below 3,000 rpm, having indistinguishable responses. However, in this case, the increasing polar moment of inertia decreases the first critical speed and its amplitude.

Comparing all the three cases, one can deduce that the damper behaviour is dependent on the location of the varying polar moment of inertia. The resonance amplitude is the most sensitive to polar moment of inertia of disk 1 and the least to that of disk 3.

5. Conclusions

The presented paper models a squeeze film damper supported flexible rotor-bearing system using Harmonic Balance Method. By introducing a predictor-corrector procedure Harmonic Balance Method is enhanced. The unbalance forced response of a three mass rotor supported on squeeze film damper at one end is investigated by varying different system parameter including, unbalance, unidirectional loads, stiffness of centering spring and gyroscopic effects of the disks. The squeeze film damper is modeled as a short bearing and the inertia effect is considered. Some concluding observations from the investigation are given below.

- The damper is found to be the most sensitive to the unbalance located on disk 2, showing the largest amplitude and hysteresis area.
- By including the unidirectional gravity loading, the orbit shape in the SFD changes dramatically, while it is displaced downward. Additionally, multi-harmonic frequency components appear in the response.
- The squeeze film damper with low centering spring stiffness can produce a well damped system, if the effect of gravity is negligible. However, the consideration of gravity results in quite different results. With soft centering spring stiffness, the more eccentric operation can introduce nonlinearity at low speeds where the effect of the unbalance force is not large enough to lift the journal more toward the journal center.
- Gyroscopic effect has a difference influence on the damper response which is dependent on the location of the gyroscopic forces along the rotor. The studied squeeze film damper response is relatively robust to the gyroscopic variations occurring within its neighborhood.

A more comprehensive model would include a finite length SFD model which renders more accurate results. This can be subject of a future work.

References

1. Gunter, E.J.; Barrett, L.E.; and Allaire, P.E. (1976). Stabilization of turbo-machinery with squeeze film dampers- theory and applications. *Institution of Mechanical Engineers Conference on Vibrations in Rotating Machinery*, Cambridge, Massachusetts, USA.
2. Dousti, S.; Kaplan, J.A.; He, F.; and Allaire, P.E. (2013). Elastomer O-rings as centering spring in squeeze film damper: Application to turbochargers. *Proceedings of ASME TurboExpo*, GT2013-94923, San Antonio, Texas, USA.
3. San Andres, L.A.; and Vance, J.M. (1987). Force coefficients for open-ended squeeze-film dampers executing small-amplitude motions about an off-center equilibrium position. *ASLE Transactions*, 30(1), 69-76.
4. Ertas, B.H.; Camatti, M.; and Mariotti, G. (2009). Synchronous response to rotor imbalance using a damped gas bearing. *Journal of Engineering for Gas Turbines and Power*, 132(3), 032501-9.
5. Taylor, D. (1980). Nonlinear response of short squeeze film dampers, *Journal of Lubrication Technology*, 102(1), 51-58.

6. Cookson, R.A.; and Kossa, S.S. (1979). The effectiveness of squeeze film damper bearings supporting rigid rotors without a centralizing spring. *International Journal of Mechanical Sciences*, 21(11), 639-650.
7. Sykes, H.; and Holmes, R. (1990). The effects of bearing misalignment on the nonlinear vibration of aeroengine rotordamper assemblies. *Proceedings of the Institution of Mechanical Engineers, Part G: Journal of Aerospace Engineering*, 204(27), 83-99.
8. Nataraj, C.; and Nelson, H.D. (1989). Periodic solutions in rotor dynamic systems with nonlinear supports: a general approach. *Journal of Vibration and Acoustics*, 111(2), 187-193.
9. Zhao, J.Y.; Linnett, I.W.; and McLean, L.J. (1994). Stability and bifurcation of unbalanced response of a squeeze film damped flexible rotor. *Journal of Tribology*, 116**(**2), 361-368.
10. Shiau, T.N.; and Jean, A.N. (1990). Prediction of periodic response of flexible mechanical systems with nonlinear characteristics. *Journal of Vibration and Acoustics*, 112(4), 501-507.
11. Hahn, E.J.; and Chen, P.Y.P. (1994). Harmonic balance analysis of general squeeze film damped multidegree-of-freedom rotor bearing systems. *Journal of Tribology*, 116(3), 499-507.
12. Bonello, P.; Brennan, M.J.; and Holmes, R. (2002). Non-linear modelling of rotor dynamic systems with squeeze film dampers an efficient integrated approach. *Journal of Sound and Vibration*, 249(4), 743-773.
13. Bonello, P.; Brennan, M.J.; and Holmes, R. (2004). The prediction of the non-linear dynamics of a squeeze-film damped aero-engine rotor housed in a flexible support structure. *Proceedings of the Institution of Mechanical Engineers, Part G: Journal of Aerospace Engineering*, 218(3), 213–230.
14. Dousti, S.; Dimond, T.W.; Allaire, P.E.; and Wood, H.E. (2013). Time transient analysis of horizontal rigid rotor supported with O-Ring sealed squeeze film damper. *Proceedings of ASME IMECE*, San Diego, California, USA.
15. Dousti, S.; and Jalali, M.A. (2013). In-plane and transverse eigenmodes of high-speed rotating composite disks. *Journal of Applied Mechanics*, 80(1), 011019.
16. San Andres, L. (2014). Force coefficients for a large clearance open ends squeeze film damper with a central feed groove: Experiments and predictions. *Tribology International*, 71, 17-25.
17. San Andres, L. (2012). Damping and inertia coefficients for two open ends squeeze film dampers with a central groove: Measurements and predictions. *Proceedings of ASME TurboExpo*, GT2012-6212.
18. Dousti, S. (2012). Realistic squeeze film damper analysis: Application of gas turbines engines. *Rotating Machinery and Controls Consortium and Annual Meeting*, Charlottesville, VA, USA.
19. Della Pietra L.; and Adiletta, G. (2002). The squeeze film damper over four decades of investigations, part I: characteristics and operating features. *Shock and Vibration Digest*, 34(1), 3-26,
20. Adiletta, G.; and Della Pietra L. (2002). The squeeze film damper over four decades of investigations, part II: rotordynamic analyses with rigid and flexible rotors. *Shock and Vibration Digest*, 34(2), 97-126.

21. Allgower, E.L.; and George, K. (1990). Numerical continuation methods. Springer, Berlin.
22. Riks, E. (1972). The application of Newton's method to the problem of elastic stability. *Journal of Applied Mechanics*, 39, 1060-1065.
23. Dousti, S.; Cao, J.; Younan, A.; Allaire, P.E.; Dimond, T.W. (2012). Temporal and convective inertia effects in plain journal bearings with eccentricity, velocity and acceleration. *Journal of Tribology*, 134, 174-184.
24. Dousti, S.; and Fittro, R. L. (2015). An extended Reynolds equation including the lubricant inertia effects: Application to finite length water lubricated bearings. *Proceedings of ASME TurboExpo*, GT2015-43826, Montreal, Canada.
25. Dousti, S.; Gerami, A.; and Dousti, M. (2016). A numerical CFD analysis on supply groove effects in high pressure, open end squeeze film dampers. *International Journal of Engineering Innovation and Research*, 5(1), 80-89.
26. Shadloo, M.S.; Poultangari, R.; Jamalabadi, M.A., and Rashidi, M.M. (2015). A new and efficient mechanism for spark ignition engines. *Energy Conversion and Management*, 96, 418-429.
27. Abdollahzadeh Jamalabadi, M.Y. (2015). Effects of micro and macro scale viscous dissipations with heat generation and local thermal non-equilibrium on thermal developing forced convection in saturated porous media. *Journal of Porous Media*, 18(9), 843-860.
28. Sakhaee-Pour, A.; Gerami, A.; and Ahmadian, A. (2008). Development of an equation to predict radial modulus of elasticity for single-walled carbon nanotubes. *Proceedings of the Institution of Mechanical Engineers, Part C: Journal of Mechanical Engineering Science*, 222(6), 1109-1115.
29. Gerami, A.; Dousti, M.; and Dousti, S. (2016). A combined structural and electromechanical approach for vibration attenuation of rotating beam. *International Journal of Engineering Innovation and Research*, 5(1), 107-113.